Quantum and classical descriptions of position and phasespace densities of a model Hamiltonian

James L. Anchell

Citation: The Journal of Chemical Physics **92**, 4342 (1990); doi: 10.1063/1.457741
View online: http://dx.doi.org/10.1063/1.457741
View Table of Contents: http://scitation.aip.org/content/aip/journal/jcp/92/7?ver=pdfcov
Published by the AIP Publishing

Quantum and classical descriptions of position and phase-space densities of a model Hamiltonian

James L. Anchell[a)]
Theoretical Chemistry Institute, University of Wisconsin, 1101 University Avenue, Madison, Wisconsin 53706

(Received 23 January 1989; accepted 28 December 1989)

Excited states of a model Hamiltonian with strongly coupled modes are investigated. Comparisons are made between the classical Poincaré surfaces of section and the Husimi function, which is a quantum mechanical phase-space density function. It is found that for the majority of states the Husimi function exhibits local maxima which resemble in shape and location the invariant tori of Poincaré surfaces of section. For certain anomalous states the maxima in the Husimi function bears no such resemblance, and these states are considered as quantum chaotic.

I. INTRODUCTION

Considerable attention has been given in recent years to try to understand the connection between classical and quantum dynamics at energies where classical chaos dominates the phase-space structure.[1–4] The purpose of this study is to compare classical and quantum phase-space descriptions of a system which demonstrates both regular and chaotic behavior. The function which gives the classical time evolution for the system of interest is the well known Pullen–Edmonds Hamiltonian[5]:

$$H(x,y,p_x,p_y) = 1/2m(p_x^2 + p_y^2) + 1/2(\omega_x x^2 + \omega_y y^2) + \lambda x^2 y^2 . \quad (1)$$

In Eq. (1) x and y are position-space variables with conjugate momenta p_x and p_y, respectively. The ω_i $(i = x,y)$ are the angular frequencies of an oscillator with mass m and coupling strength determined by λ. Throughout this paper reduced units are assumed, $(\omega_i = m = \hbar = 1)$, and $\lambda = 0.05$. With this parametrization it has been shown that for energies greater than 15 the phase space of the Pullen–Edmonds system is dominated by chaotic trajectories.[5]

A. Classical mechanics

A classical trajectory may be characterized by the number of constants of the motion restricting its propagation through phase space. For integrable systems with N degrees of freedom there are N constants of the motion. One constant is the energy, and this constrains classical trajectories to evolve on a $(2N-1)$-dimensional energy hypersurface in the $2N$-dimensional phase space. The remaining $N-1$ constants further constrain the trajectories to evolve on an N-dimensional hypertorus. Thus the trajectories of a quasi-periodic trajectory will cover the surface of a time-invariant torus. Trajectories having initial conditions which lead to nonintegrability of Hamilton's equations will have fewer than N constants of the motion. So chaotic trajectories will explore more dimensions of phase space than regular trajectories. In principle then, a chaotic trajectory of a conservative system could wander over the entire $(2N-1)$-dimensional energy hypersurface.

For systems with two degrees of freedom these trajectory types may be observed in a Poincaré surface of section.[6] The invariant tori of the regular trajectories are manifest in a surface of section as one-dimensional closed curves. Chaotic trajectories, on the other hand, will not appear as such.

B. Semi-classical mechanics

The old quantum theory offers a connection between the invariant torus of classical mechanics and the energy and state function of quantum mechanics. The Einstein–Brillouin–Keller (EBK) quantization condition[7] is given by

$$\frac{1}{2\pi}\sum_i^N \oint_C p_i dx_i = n_c + \frac{\alpha_c}{4}, \quad (2)$$

where n_c is an integer quantum number, α_c is an integer known as the Maslov index,[8,9] and C is one of the N circuits on the invariant torus. If one finds a trajectory which satisfies Eq. (2) then the energy of the state corresponds to an eigenenergy of the system. Additionally the wave function given by

$$\Psi(x_i,t) = \sum_k A_k(x_i,t)\exp[iS_k(x_i,t)] \quad (3)$$

may be evaluated by expressing the phase as

$$S_k(x_i,t) = S_k(0) + \int_0^t \sum_i p_i dx_i - Et, \quad (4)$$

and solving the equation

$$\sum_i \frac{\partial}{\partial x_i}\frac{p_i A_i^2}{m_i} = 0 . \quad (5)$$

This approximation is exact in the limit as $\hbar \to 0$.[10] Conceptually then, there is a correspondence between the invariant torus which satisfies the EBK condition imposed by Eq. (2) and the quantum eigenstate. Since the EBK condition involves a cyclic integral along a closed path C, for systems with more than one degree of freedom it can only be satisfied by quasi-periodic trajectories. A chaotic trajectory, for which no association can be made to an N-dimensional torus, cannot correspond to quantum eigenstate via the EBK formalism. Is is possible to construct a phase-space descrip-

[a)] New address: University of Utah, Chemistry Dept., Salt Lake City, UT 84112.

 0021-9606/90/074342-09$03.00

tion of a quantum system, and to observe the presence or absence of analogs to tori in this description? This is a crucial point addressed in this paper.

C. Quantum mechanics

It is difficult to define what we mean by an analog to a torus in a phase space described by quantum mechanics. First, consider that a state in quantum mechanics is represented by a vector in Hilbert space rather than as a point in phase space. It is possible however to represent a quantum state as a superposition of other quantum states, and to inquire as to the expectation value of various properties (e.g., position and momentum) of the state by measuring the expectation values of the various states in the collection. There is a double set of probabilities associated with such a measurement: first, one must know the weighting of the state in the superposition, and second, there will be an expectation value associated with the observable in that state. This measurement process is complicated by the Heisenberg uncertainty principle which asserts that it is impossible to simultaneously specify sharply the expectation values of two noncommuting observables. In the case of the position and momentum observables, this complication is minimized by representing the superposition by a collection of Gaussian wavepacket states, which allow for minimum uncertainty in both expectation values given by

$$\Delta x_i = 1/\sqrt{2}\sigma_i, \quad \Delta p_i = \sigma_i/\sqrt{2}\,, \tag{6}$$

where σ_i is the wavepacket width in the ith degree of freedom. In order to balance the uncertainty in the conjugate variables one takes $\sigma_i = 1$ for all i. For this reason σ_i has been taken equal to unity throughout this paper, and it is suppressed when there is no threat of ambiguity. The function which gives the probability of finding a state represented by a Gaussian wavepacket with expectation values $\langle \mathbf{r} \rangle = \mathbf{q}$ and $\langle \mathbf{p} \rangle = \mathbf{k}$ is the Husimi function defined by

$$\eta(\mathbf{q},\mathbf{k}) = (2\pi)^{-N/2} \langle \phi^N(\mathbf{q},\mathbf{k}) | \Gamma^N | \phi^N(\mathbf{q},\mathbf{k}) \rangle\,, \tag{7}$$

where Γ^N is the N-particle density operator and $|\phi^N(\mathbf{q},\mathbf{k})\rangle$ is an N-dimensional wavepacket state. For the present work we use the two-particle density operator, and a two-dimensional Gaussian wavepacket, which in the (x,y) representation is given by

$$\langle x,y|\phi(\mathbf{q},\mathbf{k})\rangle = \frac{(\sigma_x^2\sigma_y^2)^{1/4}}{\pi^{1/2}} \times \exp\left(-\frac{\sigma_x^2}{2}(x-q_x)^2 + ik_x x - \frac{\sigma_y^2}{2}(y-q_y)^2 + ik_y y \right). \tag{8}$$

Details concerning properties of the Husimi function may be found elsewhere.[11–14]

One further salient difference between classical and quantum phase-space concepts concerns the constraining or lack of constraining hypersurfaces in phase space. In general, the Husimi function may show a finite probability for the existence of the system anywhere in phase space—including at values of $\mathbf{q}$ and $\mathbf{k}$ which classically would be energetically inaccessible.

Due to the above considerations we will consider the quantum analog to the classical torus as a probabilistic entity. That is, we will search the quantum phase-space density defined by the Husimi function for regions of local maxima, and compare the shapes and locations of these maxima to the invariant torus which correspond semi-classically to the eigenstates of the system. The first use of the Husimi function to study the phase space of dynamical systems was carried out by Weissman and Jortner.[15]

Besides the Husimi function the Wigner function[16] gives an alternative description of phase space. A drawback of the Wigner function is that it is not necessarily strictly positive, and therefore may not be interpreted as probability density. Nevertheless researchers have successfully compared the behavior of the Wigner function to classical systems in regions of phase space characterized by either ergodic or nonergodic trajectories.[17,18]

Other related work has been carried out by Waterland *et al.*[19] Their study involved investigations of the behavior of the Husimi function for the model Hamiltonian:

$$H(x,y,p_x,p_y) = 1/2(p_x^2 + p_y^2) + 1/2x^2y^2 + [(1-\alpha)/12](x^4 + y^4)\,. \tag{9}$$

The parameter α was set to 0.95. With this parameterization the classical phase space that they studied demonstrated no quasi-periodic orbits capable of supporting an eigenstate via the EBK formalism. By comparison this paper is more concerned with the investigation of the appearance and breakdown of quantum analogs to classical tori capable of supporting eigenstates.

II. METHOD

A. Classical trajectories, position density, Husimi function

The Poincaré surfaces of section and the classical configuration-space trajectories were generated by integrating Hamilton's equations of motion using the Adams–Moulton algorithm through fifth order with variable step size.[20] For the system being studied the equations of motion are

$$\dot{x} = p_x, \quad -\dot{p}_x = x + 2\lambda x y^2,$$
$$\dot{y} = p_y, \quad -\dot{p}_y = y + 2\lambda x^2 y\,.$$

The density matrices necessary for the calculation of the quantum position-space density and of the Husimi function were obtained by diagonalizing the Hamiltonian matrix with a distributed Gaussian basis set.[21–23] That is, a primitive basis set was constructed from a square grid of Gaussians distributed throughout position space. The unnormalized Gaussians are expressed as

$$g_i(x) = \exp[-\alpha_i(x-x_i)^2]\,, \tag{10}$$

where α_i is the Gaussian width and x_i is the location of the Gaussian center. The grid was constructed in the following manner. Along the x axis $2N+1$ Gaussians were distributed with N Gaussians on the positive x axis; N Gaussians on the negative x axis, and one Gaussian at the origin. This primitive set of functions was labeled

$$g_{-N}(x), g_{-N+1}(x), \ldots, g_0(x), \ldots, g_{N-1}(x), g_N(x) . \quad (11)$$

It was found that taking $N = 24$ was computationally tractable and gave satisfactory convergence to the states studied. On the positive and negative axes the spacing between Gaussians was 0.25 from ± 0.25 to ± 0.50, and 0.50 from ± 0.55 to ± 0.7. The Gaussians labeled with negative indices were centered between $g_{-N}(x)$ and $g_0(x)$, and the Gaussians labeled with positive indices were centered between $g_0(x)$ and $g_N(x)$. In practice the number of Gaussians should be greater than the number of nodes in the highest energy wave function whose convergence is desired. In order to allow for tunneling into the potential barrier, Gaussians should be centered beyond the classical turning point given by a distance $\sqrt{2E}$, where E is the energy of this most highly excited state. It was found that choosing $\alpha_0 = 0.5$ and the remaining α_i so that the overlap between adjacent Gaussians was equal to 0.9 gave good convergence to the energies. From this initial set of functions an intermediate set of odd and even functions in x was constructed. These functions labeled $\tilde{\phi}_i^e(x)$ and $\tilde{\phi}_i^o(x)$ were given by

$$\begin{aligned} &\tilde{\phi}_0^e(x) = g_0(x) \\ &\tilde{\phi}_i^e(x) = g_i(x) + g_{-i}(x) \\ &\tilde{\phi}_i^o(x) = g_i(x) - g_{-i}(x), \quad i = 1,2,\ldots N. \end{aligned} \quad (12)$$

The even and odd functions were then symmetrically orthogonalized[24] to form a set of functions designated $\phi_i^e(x)$ and $\phi_i^o(x)$. From these one-dimensional orthonormal functions, symmetry-adapted basis functions with two degrees of freedom were constructed. In the present example $\omega_x = \omega_y$, so the symmetry group of the Pullen–Edmonds Hamiltonian is isomorphic to the C_{4v} point group. The symmetry-adapted basis set pertaining to the one-dimensional irreducible representations of C_{4v} are given by

$$A_1: \quad \psi_{mn}(x,y) = \begin{cases} 2^{-1/2}[\phi_m^e(x)\phi_n^e(y) + \phi_n^e(x)\phi_m^e(y)] & m \neq n \\ \phi_m(x)\phi_n(y) & m = n \end{cases} \quad (13)$$

$$A_2: \quad \psi_{mn}(x,y) = 2^{-1/2}[\phi_m^o(x)\phi_n^o(y) - \phi_n^o(x)\phi_m^o(y)] \quad m \neq n \quad (14)$$

$$B_1: \quad \psi_{mn}(x,y) = 2^{-1/2}[\phi_m^e(x)\phi_n^e(y) - \phi_n^e(x)\phi_m^e(y)] \quad m \neq n \quad (15)$$

$$B_2: \quad \psi_{mn}(x,y) = \begin{cases} 2^{-1/2}[\phi_m^o(x)\phi_n^o(y) + \phi_n^o(x)\phi_m^o(y)] & m \neq n \\ \phi_m^o(x)\phi_n^o(y) & m = n \end{cases} \quad (16)$$

For this study only the A_1 symmetry states were considered.

The Husimi function and the position density were evaluated in the following way. The two-particle density matrix corresponding to a particular vibrational eigenstate of the system is given by

$$\Gamma^i(x,y|x',y') = \Psi_i(x,y)\Psi_i^*(x',y') , \quad (17)$$

where $\Psi_i(x,y)$ is an eigenstate of the Hamiltonian. The two-particle density is obtained by setting $x = x'$ and $y = y'$ in Eq. (17), and the Husimi function may be evaluated by the substitution of Eq. (17) into Eq. (7):

$$\eta(\mathbf{q},\mathbf{k}) = (1/2\pi)F_i(q_x,q_y,k_x,k_y)F_i^*(q_x,q_y,k_x,k_y) . \quad (18)$$

In Eq. (18) $F_i(q_x,q_y,k_x,k_y)$ is the overlap between a two-degree-of-freedom Gaussian wavepacket and the ith eigenstate of the system:

$$F_i(q_x,q_y,k_x,k_y) = \iint \Psi_i^*(x,y)\phi(q_x,k_x|x) \times \phi(q_y,k_y|y)dxdy . \quad (19)$$

In the basis chosen for this study, $\Psi_i(x,y)$ can ultimately be expressed as a linear combination of products of distributed Gaussians. That is,

$$\Psi_i(x,y) = \sum_{i=-N}^{N} \sum_{j=-N}^{N} T_{ij} g_i(x) g_j(y) , \quad (20)$$

where T_{ij} is an expansion coefficient which represents the multiple transformations from distributed Gaussians to odd and even functions, then to normalized functions, then to symmetrized functions, and finally to eigenvectors of the Hamiltonian. Substitution of Eq. (20) into Eq. (19) yields

$$F_i(q_x,q_y,k_x k_y) = \sum_{i=-N}^{N} \sum_{j=-N}^{N} T_{ij} f_i(q_x,k_x) f_j(q_y,k_y) , \quad (21)$$

where $f_i(q_x,k_x)$ is the overlap between a Gaussian wavepacket and a distributed Gaussian:

$$f_i(q_x,k_x) = \int g_i^*(x)\phi(q_x,k_x|x)dx . \quad (22)$$

The integral appearing in Eq. (22) has an analytical expression given elsewhere.[13]

B. Adiabatic approximation

Moiseyev and Weinhold,[25] hereafter referred to as (MW), have recently devised a numerical method for assigning approximately good quantum numbers to the Pullen–Edmonds states. Their goal is to establish a pattern between the nearly good quantum numbers and chaotic energy regions—as in, for example, regions of multiple avoided crossings.[26] Their intermediate results are of value to this research. A summary of their method is as follows. First, the essentially exact eigenstates of the Hamiltonian were determined via a variational calculation using a basis set consisting of symmetrized products of harmonic oscillator basis functions. That is, the eigenstates were represented as

$$\Psi^i(x,y) = \sum_{m \geq n} C_{mn}^i \Phi_{mn}(x,y) , \quad (23)$$

where

$$\Phi_{mn}(x,y) = \begin{cases} \sqrt{\frac{1}{2}}[\psi_m(x)\psi_n(y) + \psi_n(x)\psi_m(y)] & m \neq n \\ \psi_m(x)\psi_n(y) & m = n \end{cases} . \quad (24)$$

In Eqs. (24) and (23) $\psi_m(x)$ is a harmonic oscillator eigenstate and C_{mn}^i is an element of the ith eigenvector obtained by diagonalizing the Hamiltonian. The calculation employed 200 of these product basis functions. The next step

was to calculate the eigenvectors and eigenvalues in the adiabatic approximation. That is, one assumes a form of the wave function given by

$$\Psi^{\rm ad}_{mn}(x,y) = \varphi_m(y)\chi_n(x;y). \tag{25}$$

Substitution of Eq. (25) into the Schrödinger equation and ignoring the kinetic energy term $\mathbf{p}_y^2\chi_n(x;y)$ leads to a set of coupled adiabatic eigenvalue equations. Details may be found in Ref. 28. The result is a state function with good quantum numbers m and n, where m labels the energy level in the x degree of freedom and n labels the energy level in the y degree of freedom. The crucial question is: Is the state function thus obtained a good representation of an exact eigenfunction of the Hamiltonian? If so, then we assert that the numbers m and n are approximately good quantum numbers to that eigenstate. The quality of the adiabatic wave function was measured by calculating the square of its overlap, d_i, with one of the three variational wave functions closest in energy to it:

$$d_i = \left(\int \Psi^{\rm ad}_{mn}(x,y)\Psi_i(x,y)dxdy \right)^2 . \tag{26}$$

The state function with the greatest value of d_i received the label whose goodness may be measured from the magnitude of d_i. The results obtained for the first 62 adiabatic state functions are given in Table I.[25] Since the adiabatic state function was not symmetrized, values of d_i close to 0.5 when $m \neq n$ represent excellent overlap.

III. RESULTS

Figure 1 shows the quantum position densities of the 21st, 29th, and 34th states of A_1 symmetry of the coupled oscillators, respectively. For almost every state studied, the shape of the density in configuration space resembles either a plus (+) or a cross (×). For example the 29th and 34th

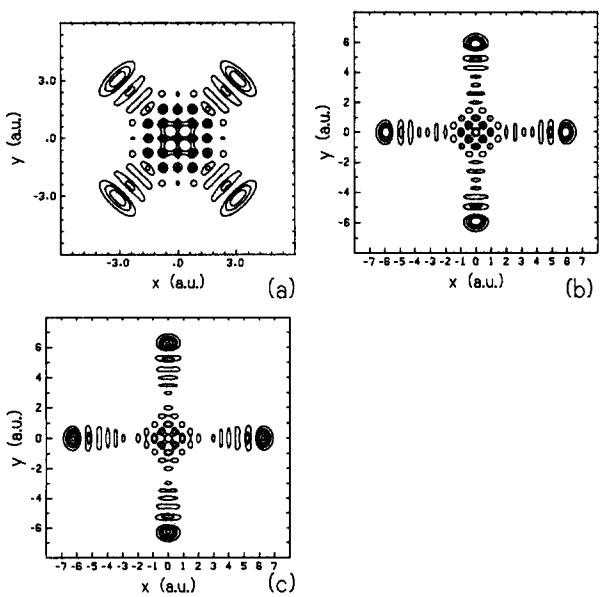

FIG. 1. Coordinate density for (a) 21st, (b) 29th, (c) 34th A_1 symmetry adapted states. Contours: (a) 0.02–0.12 in steps of 0.02, (b) 0.02–0.08 in steps of 0.02, (c) 0.02–0.10 in steps of 0.02.

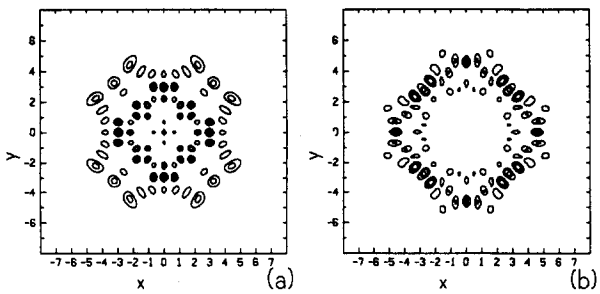

FIG. 2. Coordinate density for (a) 30th and (b) 33rd A_1 symmetry-adapted states. Contours: (a), (b) 0.02–0.08 in steps of 0.02.

states have a plus-shaped density, and the 21st state has a density best described as a cross. The position densities of the 30th and 33rd states shown in Fig. 2 are presented here as exceptions to this observation. The density of these states do weakly resemble either a plus (30th state) or a cross (33rd state), but the density is less localized about these shapes.

In *some* cases one can predict from the labeling scheme of MW which of these classes of shapes the position density for a given state will demonstrate. If a state is labeled with (m,n) such that $n \gg m$, then the state is characterized by high excitation in the x mode, and relatively low energy in the y mode. One would expect the density to be elongated along the x axis, and narrow along the y axis. Upon symmetrization, the resulting density resembles the plus shape. The same will hold true if $m \gg n$. If $m \approx n$ then the energy in the two modes is nearly equal, and upon symmetrization a cross-shaped density appears. For simplicity, we will refer to these conditions (i.e., $n \gg m$, $m \gg n$, or $m \approx n$) as the *mn* conditions. It will be shown later that states satisfying the *mn* condition correspond to states which are easily related to a trajectory quantized on an invariant torus. In the search for unusual eigenstates to study, the chance for success is better if one steers clear of states with good overlap to an adiabatic state satisfying the *mn* condition. One must be careful here, as DeLeon, *et al.*[27] have shown that many states which at first glance appear to be unusual (e.g., demonstrating unusual nodal structure) are often quantizable on trajectories having nonlinear resonances. At low energies it is hard to find an eigenstate which violates the *mn* condition. For example, one might consider the state labeled (3,7) to be a good candidate. However, examination of Table I reveals that this state also has good overlap with the (6,4) and (5,5) adiabatic states. The 30th and 33rd states were chosen for study because they apear to violate the *mn* condition. The 30th state only weakly violates the *mn* condition. For although it is labeled by the (8,3) and (4,7) quantum numbers, it also has fair overlap with the adiabatic state labeled (6,5). The 33rd state is a good candidate as a nonsubscriber to the (m,n) condition, as this state is labeled by only one set of quantum numbers (3,9).

Figure 3 shows Poincaré surfaces of section at energies which match those of the 21st and 30th states. All the sections were taken in $x - p_x$ space with $y = 0$. The basic features of sections taken at nearby energies (as, for example, energies corresponding to the 29th, 33rd, and 34th eigen-

TABLE I. Overlap between the adiabatic and the A_1 symmetry adapted variational wave functions. n,m denote the energy levels of the x and y modes, respectively, and d denotes the square of the overlap. E_{ex}, E_{ad}, and E_{dg} refer to the exact, adiabatic, and distributed Gaussian energies (from Ref. 17).

State	(m,n)	E_{ex}	E_{ad}	E_{dg}	d
1	(1,1)	1.012 07	1.011 95	1.012 07	1.00
2	(1,2)	3.079 64	3.056 95	3.079 64	0.49
2	(2,1)	3.079 64	3.057 31	3.079 64	0.51
3	(1,3)	5.075 34	5.097 47	5.075 34	0.46
3	(3,1)	5.075 34	5.099 40	5.075 34	0.44
4	(2,2)	5.302 06	5.274 49	5.302 06	0.89
5	(1,4)	7.126 81	7.134 71	7.126 81	0.49
5	(4,1)	7.126 81	7.138 84	7.126 81	0.48
6	(2,3)	7.607 22	7.471 82	7.607 22	0.44
6	(3,2)	7.607 22	7.477 88	7.607 22	0.53
7	(1,5)	9.154 84	9.169 40	9.154 84	0.48
7	(5,1)	9.154 84	9.176 06	9.154 84	0.46
8	(2,4)	9.516 61	9.654 17	9.516 61	0.36
8	(4,2)	9.516 61	9.669 48	9.516 61	0.25
9	(3,3)	10.013 29	9.824 29	10.013 29	0.63
10	(1,6)	11.189 30	11.202 01	11.189 30	0.49
10	(6,1)	11.189 30	11.212 40	11.189 30	0.47
11	(2,5)	11.792 06	11.824 63	11.792 06	0.46
11	(5,2)	11.792 06	11.851 06	11.792 06	0.38
12	(3,4)	12.504 32	12.145 91	12.504 32	0.37
12	(4,3)	12.504 32	12.158 10	12.504 32	0.50
13	(1,7)	13.220 14	13.232 90	13.220 17	0.49
14	(2,6)	13.855 82	13.985 36	13.855 82	0.33
14	(6,2)	13.855 82	14.024 01	13.855 82	0.22
15	(3,5)	14.244 78	14.447 58	14.244 78	0.22
16	(5,3)	15.074 86	14.475 79	15.074 86	0.30
15	(4,4)	14.244 78	14.613 63	14.244 78	0.34
17	(1,8)	15.250 40	15.262 32	15.250 56	0.49
17	(8,1)	15.250 40	15.277 39	15.250 56	0.47
18	(2,7)	16.057 44	16.137 90	16.057 45	0.42
19	(3,6)	16.735 00	16.732 72	16.735 00	0.38
19	(6,3)	16.735 00	16.779 40	16.735 00	0.19
21	(4,5)	17.718 91	17.042 18	17.718 91	0.30
21	(5,4)	17.718 91	17.060 32	17.718 91	0.45
20	(1,9)	17.279 59	17.290 48	17.280 09	0.49
20	(9,1)	17.279 59	17.308 42	17,280 09	0.47
22	(2,8)	18.192 01	18.283 43	18.192 08	0.41
22	(8,2)	18.192 01	18.348 19	18.192 08	0.29
25	(3,7)	19.316 82	19.003 85	19.316 85	0.21
24	(1,10)	19.306 33	19.317 53	19.306 49	0.42
24	(10,1)	19.306 33	19.338 33	19.306 49	0.40
25	(4,6)	19.316 82	19.448 16	19.316 85	0.10
25	(6,4)	19.316 82	19.488 42	19.316 85	0.003
25	(5,5)	19.316 82	19.611 70	19.316 85	0.20
26	(2,9)	20.343 80	20.422 87	20.344 14	0.44
26	(9,2)	20.343 80	19.501 04	20.344 14	0.30
28	(3,8)	21.106 50	21.262 92	21.106 60	0.32
29	(1,11)	21.336 01	21.343 59	21.337 72	0.49
30	(8,3)	21.960 43	21.350 68	21.960 47	0.22
29	(11,1)	21.336 01	21.367 23	21.337 72	0.47
30	(4,7)	21.960 43	21.834 89	21.960 47	0.30
30	(5,6)	21.960 43	22.135 12	21.960 47	0.01
30	(6,5)	21.960 43	22.158 85	21.960 47	0.20
31	(2,10)	22.483 57	22.556 95	22.484 24	0.44
31	(10,2)	22.483 57	22.648 57	22.484 24	0.30
34	(1,12)	23.363 66	23.368 77	23.373 03	0.46
34	(12,1)	23.363 66	23.395 21	23.373 03	0.46
33	(3,9)	23.249 91	23.511.44	23.250 13	0.20
35	(9,3)	23.739 04	23.620 86	23.739 18	0.13
37	(4,8)	24.675 64	12.204 92	24.675 77	0.24
37	(8,4)	24.675 64	24.296 67	24.675 77	0.13
35	(5,7)	23.739 04	24.634 52	23.739 18	0.23

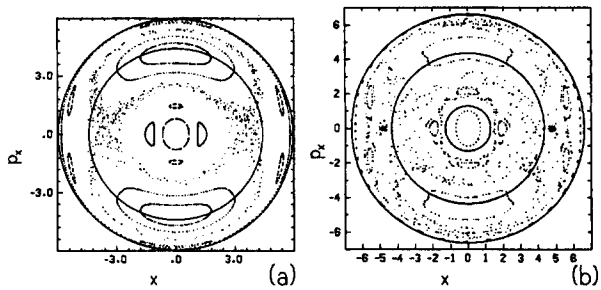

FIG. 3. Poincaré surfaces of section at energies equal to the energy of the (a) 21st, (b) 30th A_1 symmetry states. The solid circles in (a) correspond to constant values of p_y equal to 0 and 4 for the outer and inner curves, respectively. The solid circles in (b) correspond to constant values of p_y equal to 0, 5, and 6.5 for the outer, middle, and inner curves, respectively.

states) are typified in these two figures. For a system of uncoupled oscillators the surfaces of section would show concentric ellipses associated with different energies. The coupling, however, gives rise to the resonances which are centered at nonzero values of x and/or p_x. The large resonances centered roughly at $x = 0$ and $p_x = \pm 4$ are 1:1 resonances. The smaller islands scattered throughout the energetically available phase space correspond to higher order resonances such as 2:1 or 3:2, etc. As either the coupling or the energy is increased the extent of these resonance zones increases. If the energy or coupling is increased to the extent that two or more of these resonances overlap then the tori associated with these sections breakup and the trajectories generating them become one chaotic trajectory.[29,30] Furthermore, as these parameters are increased, so is the degree to which the chaotic trajectories dominate phase space.

Many of the structures of the Poincaré surface of section are related through the symmetry of the Hamiltonian. By applying the symmetry operators of the C_{4v} point group, reflection and inversion, to the initial conditions of a given quasi-periodic trajectory, a symmetry-related partner may be generated. For example, if one knows the initial conditions leading to a trajectory describing the large outer circular section concentric about the origin, a symmetry-related inner section may be generated by letting $(x^0,y^0) \rightarrow (y^0,x^0)$ and $(p_x^0,p_y^0) \rightarrow (p_y^0,p_x^0)$. Similarly, types of relationships hold for the resonances. These symmetry-related tori give us information as to the behavior of the system in the other degrees of freedom. For example, a trajectory describing an inner circle in an x-p_x section will simultaneously create the symmetry-related larger outer circle in the y-p_y section. Similarly, the 1:1 resonance islands will appear exactly the same in the y-p_y frame as in the x-p_x frame. For chaotic trajectories applying the symmetry operations to the initial conditions does not lead to a symmetry-related partner located elsewhere in a two-dimensional phase-space section. The symmetry-related sections represent cross sections of separate time-propagated classical states which differ in their initial conditions. In quantum mechanics the initial conditions are contained in the phase of the wave function, so that knowledge of the initial conditions of a state are lost in the calculation of physical quantities. Symmetry partners, therefore, are not present in the quantum mechani-

cal phase-space description of the density. As we shall see later the phase-space density of a quantum state appears to include simultaneously all of the symmetry-related tori.

A useful feature of this Hamiltonian is its functional value of p_y when $y = 0$. In this case we have

$$p_y = (2E - p_x^2 - x^2)^{1/2} . \tag{27}$$

For any of the surfaces of section shown in this paper constant values of p_y lie upon concentric circles. Some of these constant values of p_y are indicated in Fig. 3. Although the system has four degrees of freedom the above-mentioned considerations allow the observer to develop a good understanding of the behavior of the system in all its dimensions while examining a section in only two dimensions.

The configuration-space trajectories corresponding to the gross features of the phase-space cross sections are simple in nature. The inner, round section corresponds to small amplitude motion in the x-degree of freedom and large amplitude motion in the y direction. Conversely, the large, outer, and round symmetry-related cross section corresponds to a rotation of this trajectory by $\pi/2$ radians. That is, the trajectory has large amplitude motion in the x mode and small amplitude motion in the y mode. The configuration-space trajectories corresponding to 1:1 resonance zones have nearly equal amounts of energy in both modes. These trajectories roughly bisect the x and y axes. A class of chaotic trajectories arises when at high enough energies some of these displaced islands begin to overlap and breakup. An example of this type of chaos may be seen in Fig. 3(a). In x-p_x space these trajectories fill a region similar to that occupied by the displaced islands, but they are much less localized. When the higher order resonance zones begin to break up, a second class of chaotic trajectory appears. The region filled by this second class of chaotic trajectory viewed in x-p_x space is ring-like in structure. One ring may be found just inside the turning point boundary, and the other may be found at a radius somewhat greater than the radius surrounding the bundle of regular trajectories in the center of surface of section. This second type of chaos may be seen in Fig. 3(b) along with the first type discussed. Examples of some of these trajectories are shown in Figs. 4 and 5.

As with the Poincaré surface of section we evaluate the Husimi function by considering its cross section in q_x-k_x space evaluated at $q_y = 0$. Furthermore the value of k_y is set

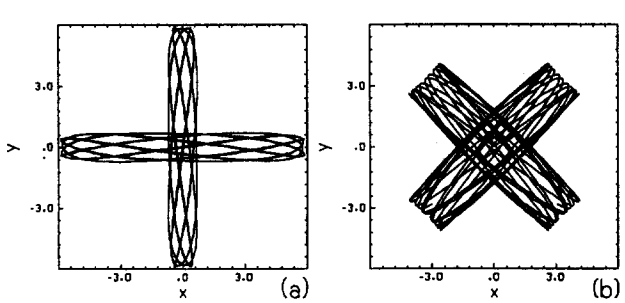

FIG. 4. Superimposed, symmetry-related configuration space trajectories corresponding to features of the Poincaré surfaces of section shown in Fig. 3. (a) Corresponds to inner and outer rings. (b) Corresponds to 1:1 resonance zones.

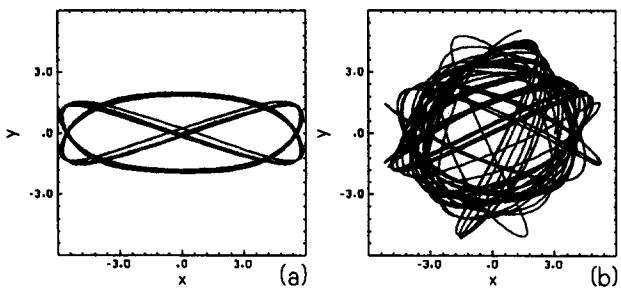

FIG. 5. Configuration space trajectories of (a) a 2:3 resonance, (b) a chaotic trajectory.

so that it satisfies the relationship given in Eq. (27). With these restraints we know that the phase-space density of the Husimi function should converge to the classical phase-space density in the limit as $\hbar$ goes to zero. There are two qualities of the Husimi function which will be important to note in the following analyses. First, the relative position and shape of the Husimi function compared to the tori sections observed in classical phase space. Second, the degree of nonlocality of the Husimi function. The degree of locality may be observed by plotting two sets of contours per figure. One set will have values the same order of magnitude as the peak heights in the Husimi function. The second set of contours will be one order of magnitude smaller; these will be indicated with dashed lines. For highly localized density the second set of contours should merely outline the first set—not giving new information regarding the shape and extent of the function. For a nonlocal density the second set of contours will wander over a great deal more of the available phase space; the function will appear flatter and more spread out. Berry[31] has suggested that the Wigner distribution corresponding to chaotic states should appear relatively flat. As the Husimi function is a Gaussian convolution of the Wigner function the same should hold true for it.

Consider first the 21st A_1 symmetry-adapted state. The Husimi function for this state is shown in Fig. 6. The peak

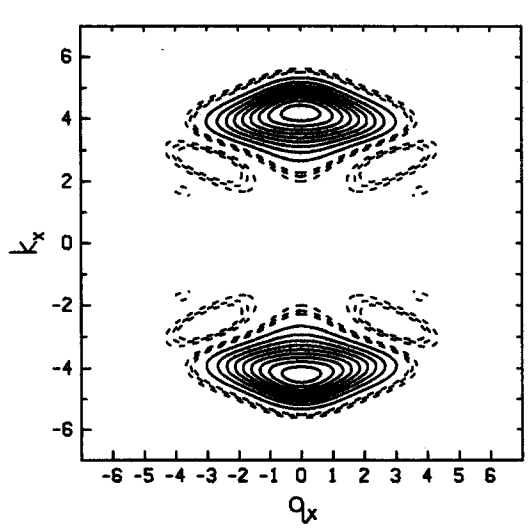

FIG. 6. Husimi function section for 21st A_1 symmetry-adapted state. Solid lines: 0.001–0.004 in steps of 0.001. Dashed lines: 0.0001–0.0003 in steps of 0.0001.

values in the quantum phase-space density in this case resemble the large, symmetry-related upper and lower islands of the Poincaré surface of section. One observes that the trajectory types which correspond to this feature of the surface of section roughly bisect the x and y axes, and that the cross-shaped quantum mechanical position-space density of this state does likewise. The smaller contours in Fig. 6 do slightly alter the overall shape of the phase-space density, but do not indicate any large degree of nonlocality.

The 29th A_1 symmetry-adapted state is considered next. The Husimi function for this state is shown in Fig. 7. The density unmistakably resembles the large outer ring, and its complement the inner ring which appears in a Poincaré surface of section. These trajectories correspond to motion whose amplitude is large in one degree of freedom and small in the other (see Fig. 4.) This is also consistent with quantum mechanical position density shown in Fig. 1 which is plus shaped. The density is very local; the smaller contours only outline the peak density.

Next consider the 30th state, which as we saw before weakly violated the mn condition. The Husimi function for this state is shown in Fig. 8. The density covers the classical region occupied by the 1:1 resonance zone and some of the classically chaotic space. The delocalization of this state appears more significant than in the previous two states. However, some doubt is cast onto the supposition that this state in some way corresponds to a classically chaotic trajectory, as there is little buildup in density in the separatrix region, which is the region most densely filled with chaotic trajectories in the classical picture.

The 33rd state is one of the most intriguing of those studied. The quantum phase-space density for this function is shown in Fig. 9. At first it appears to form a ring like the one observed for the 21st state. However, it is unlikely to correspond to a quasi-periodic trajectory like the one described for state 21 for the following reasons: (a) the ring is

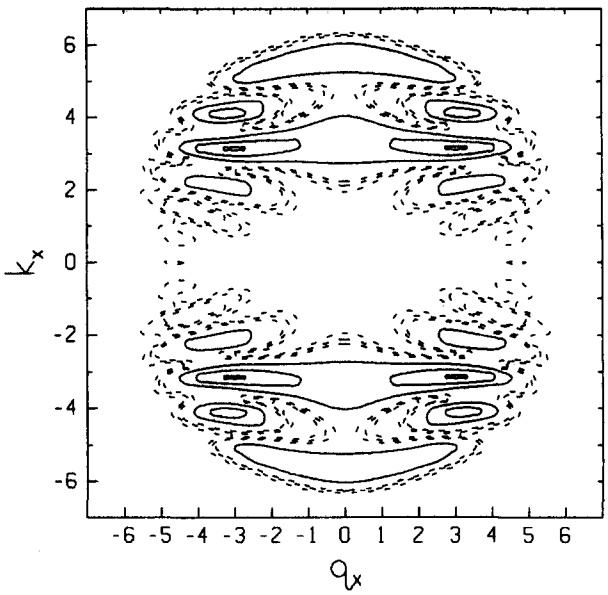

FIG. 8. Husimi function section for 30th A_1 symmetry-adapted state. Solid lines: 0.001–0.004 in steps of 0.001. Dashed lines: 0.0001–0.0003 in steps of 0.0001.

only formed after the addition of contours one order of magnitude smaller than the contours corresponding to the contour values giving the peak height; (b) no probability density appears near the inner turning point where the symmetry partner should be; and (c) the ring is actually slightly inside the classical turning point boundary and not on it, as in the previous case. In fact, the density is built-up in the regions which appear classically chaotic, and avoids those regions which are quasiperiodic. In particular, the peak in the density is in the separatrix region where the largest degree of chaos is observed in the classical surface of section. The addition of the smaller contours reveals a phase-

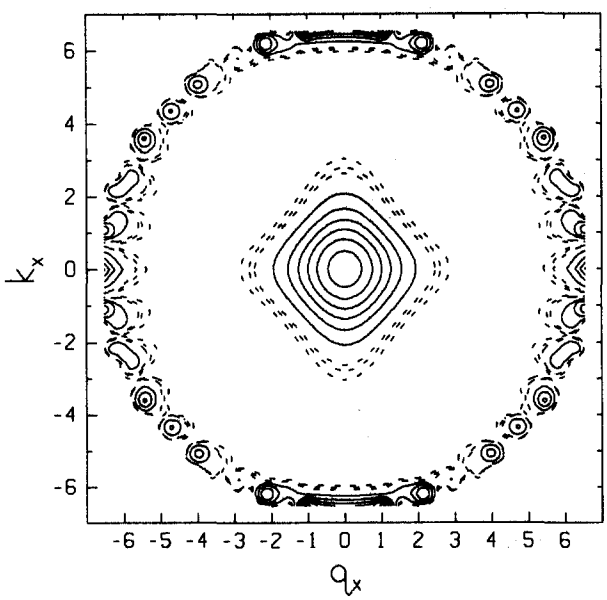

FIG. 7. Husimi function section for 29th A_1 symmetry-adapted state. Solid lines: 0.001–0.006 in steps of 0.001. Dashed lines: 0.0001–0.0003 in steps of 0.0001.

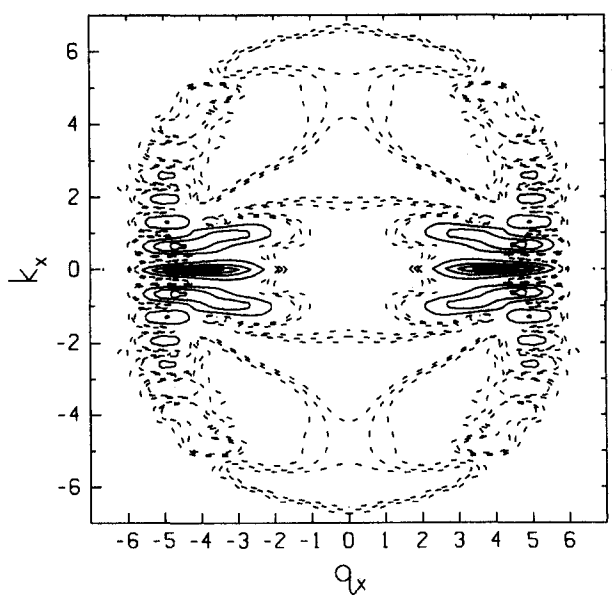

FIG. 9. Husimi function section for 33rd A_1 symmetry-adapted state. Solid lines: 0.001–0.004 in steps of 0.001. Dashed lines: 0.0001–0.0003 in steps of 0.0001.

space density which is *extremely* delocalized. Eigenstate 33 corresponds in shape nicely to a classically chaotic trajectory which arises from the breakup of some of the higher order resonance zones. This is supported by the adiabatic labeling of the state (3,9), which suggest a correspondence to a classical trajectory possessing a 1:3 resonance.

The last state studied, 34, is only slightly higher in energy than the 33rd state. Its character is however markedly different. Labeled strongly as a (12,1) or (1,12) state, the position density shows a strong plus shape. The quantum phase-space density for this function is shown in Fig. 10. The analysis of this state is similar to that given for the 29th eigenstate.

IV. DISCUSSION

It has been observed from the Poincaré surfaces of section that there are two major classes of trajectory capable of supporting a quantum eigenstate via the EBK condition. The first class involves trajectories whose caustics in configuration space are parallel to the x and y axes. The Poincaré sections for these trajectories are characterized by sections which are roughly circular and centered about the origin. The second class of trajectories have caustics which are roughly at 45° angles to the x and y axes. The Poincaré sections for these trajectories are characterized by closed curves which are displaced from the origin and have a mirror image through the x axis. Similarly, two classes of quantum eigenstates were observed: one having plus-shaped density and the other having cross-shaped density. One expects from symmetry that the first class of classical trajectories should correspond to eigenfunctions with plus-shaped densities, and the second class of trajectories should correspond to eigenfunctions with cross-shaped densities.

Eigenstates 29 and 34 have plus-shaped densities which are akin to the space filled from a combination of trajectories corresponding to the inner and outer ring regions of the Poincaré surfaces of section. Eigenstate number 21 has a cross-shaped density which resembles a mix of trajectories which correspond to the large upper and lower displaced islands in the surfaces of section. For these states, the Husimi function demonstrated local maxima which compared to the above-mentioned tori sections in both shape and location. Classically, these quasi-periodic trajectories are dynamically isolated from one another. That is, a trajectory which starts out on one periodic or quasi-periodic orbit will never end up in another. Nevertheless, Davis and Heller[32] have shown that for a modified Barbanis potential[33] quantization of combined symmetry-related trajectories leads to good representations of the wave function. Other eigenstates besides those presented here were studied. Their analysis was similar to the eigenstates discussed above, i.e., the eigenstates appeared to correspond in an obvious way to one of the two major classes of the quasi-periodic trajectories.

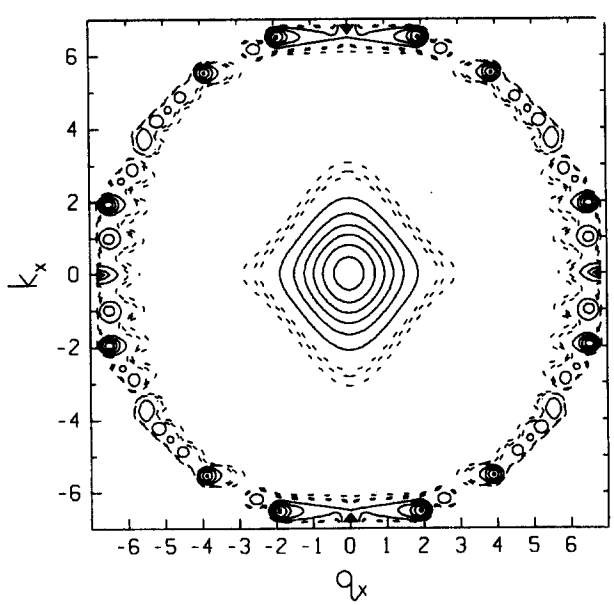

FIG. 10. Husimi function section for 34th A_1 symmetry-adapted state. Solid lines: 0.001–0.006 in steps of 0.001. Dashed lines: 0.0001–0.0003 in steps of 0.0001.

Two exceptions were found in states 30 and 33. The quantum phase-space density of state 30 resembles the region of classical phase space occupied by a 1:1 resonance zone. However, the phase-space density also shows considerable buildup in regions which are classically chaotic. Although the state is relatively nonlocal, the absence of density in the separatrix region suggests that this state does not correspond to a classical chaotic trajectory. The phase-space density of eigenstate 33 not only occupies regions of phase space which are classically chaotic, but it avoids those regions occupied by regular trajectories. Furthermore, this state demonstrates a sizeable buildup of density in the separatrix region, and also exhibits an exceptional degree of nonlocality. This unusual buildup of density in the separatrix region has been observed elsewhere using the Wigner function to represent the quantum phase-space density.[18] These observations coupled with the state's adiabatic label (3,9) lead one to suspect that this quantum state is associated with a classically chaotic trajectory arising from the breakup of a 1:3 resonance zone.

This work is of a qualitative nature and quantitative work should be carried out to substantiate that there is a correspondence of some of the Pullen–Edmond's states to chaotic trajectories. The EBK condition does not allow for the quantization of irregular trajectories. However other methods of quantizing classical trajectories have been developed.[3] In particular, the adiabatic switching method described by Skodje *et al.* provides a technique which has been used to successfully quantize chaotic trajectories.[34]

The adiabatic labeling of the states provides a tool to speed up the search of the many possible states of the spectrum for possible deviations from semi-classical correspondence to regular trajectories. Classically, the critical energy at which the Pullen–Edmonds Hamiltonian becomes dominated by chaotic trajectories is around $E_c = 15$. However, most of the eigenstates studied whose energy was above E_c corresponded nicely to regular classical trajectories. The observation that chaotic effects appear at higher energies in the quantum mechanical description than in the classical description has been noted elsewhere.[35,36] This phenomenon arises because the Husimi function smooths out the finer structures of classical phase space. Its maximum resolution

is over an area with dimensions $\hbar$, so that the chaotic zones must grow at least to this order of magnitude before chaotic effects can be observed.

It is interesting to note that eigenstate number 33 which is very close in energy to eigenstate 34 has vastly different one-particle densities from state 34. And even though the latter was higher in energy it appears to correspond nicely to a regular trajectory while the former does not. At higher energies the density of states not satisfying the mn condition increases. So that if the supposition that these states are good candidates for quantum chaos is correct then there is an analogy to classical mechanics in which the ratio of the number of chaotic to regular trajectories increases with energy.

ACKNOWLEDGMENTS

The author is grateful to several people who assisted with many phases of this project. In particular, thanks go to Edwin Sibert, Daniel Colbert, John Harriman, Frank Weinhold, Nimrod Moiseyev, and Rudolph Mayrhofer, all of whom provided valuable advice, insight, and support. The work reported in this paper was supported by the National Science Foundation through Grant No. CHE-8519723.

[1]S. A. Rice, Adv. Chem. Phys. **47**, 117 (1981).
[2]P. Brumer, Adv. Chem. Phys. **47**, 201 (1981).
[3]D. W. Noid, M. L. Koszykowski, and R. A. Marcus, Annu. Rev. Phys. Chem. **32**, 267 (1981).
[4]E. B. Stechel and E. J. Heller, Annu. Rev. Phys. Chem. **35**, 563 (1984).
[5]R. A. Pullen and A. R. Edmonds, J. Phys. A **14**, 1477 (1981).
[6]H. Poincare, *New Methods of Celestial Mechanics* (Transl. NASA, Washington DC, 1967), Vol. 3, Chap. 27.
[7]J. Keller, Ann. Phys. **4**, 180 (1958).
[8]V. Maslov, *Théorie des Perturbations* (Dunod, Paris, 1972).
[9]I. C. Percival, Adv. Chem. Phys. **36**, 1 (1977).
[10]P. A. M. Dirac, *The Principles of Quantum Mechanics*, 4th ed. (Oxford University, London, 1958), p. 121.
[11]K. Husimi, Proc. Phys. Math Soc. Jpn. **22**, 264 (1940).
[12]M. E. Casida, J. E. Harriman, and J. L. Anchell, Int. J. Quantum Chem. Quantum Chem. Symp. **21**, 435 (1987).
[13]J. E. Harriman, J. Chem. Phys. **88**, 6399 (1988).
[14]J. L. Anchell and J. E. Harriman, J. Chem. Phys. **89**, 6860 (1988).
[15]Y. Weissman and J. Jortner, Chem. Phys. **77**, 1486 (1982).
[16]E. Wigner, Phys. Rev. **40**, 749 (1932).
[17]J. S. Hutchinson and R. E. Wyatt, Phys. Rev. A **23**, 1567 (1980).
[18]M. J. Davis, J. Phys. Chem. **92**, 3124 (1988).
[19]R. L. Waterland, J. Min Yuan, C. C. Martens, R. E. Gillilan, and W. P. Reinhardt, Phys. Rev. Lett. **61**, 2733 (1988).
[20]R. L. Burden, J. D. Faires, and A. C. Reynolds, *Numerical Analysis*, 2nd ed. (Prindle, Weber, and Schmidt, Boston, 1981).
[21]I. P. Hamilton and J. C. Light, J. Chem. Phys. **84**, 306 (1986).
[22]Z. Bačić, P. Watt, and J. C. Light, J. Chem. Phys. **89**, 947 (1988).
[23]R. M. Whitnell and J. C. Light, J. Chem. Phys. **89**, 3674 (1988).
[24]P. O. Löwdin, J. Chem. Phys. **18**, 365 (1950).
[25]N. Moiseyev and F. Weinhold (work in progress).
[26]R. A. Marcus, in *Horizons of Quantum Chemistry*, edited by K. Fukui and B. Pullman (Reidel, Boston, 1980).
[27]N. DeLeon, M. J. Davis, and E. J. Heller, J. Chem. Phys. **80**, 794 (1984).
[28]P. R. Certain and N. Moiseyev, J. Chem. Phys. **86**, 2146 (1986).
[29]G. H. Walker and J. Ford, Phys. Rev. **188**, 416 (1969).
[30]B. V. Chirikov, Phys. Rep. **52**, 265 (1979).
[31]M. V. Berry, J. Phys. A **10**, 2083 (1977).
[32]M. J. Davis and E. J. Heller, J. Chem. Phys. **75**, 246 (1981).
[33]B. Barbanis, Astron. J. **71**, 415 (1966).
[34]R. T. Skodje, F. Borondo, and W. P. Reinhardt, J. Chem. Phys. **82**, 4611 (1985).
[35]E. J. Heller, J. Chem. Phys. **72**, 1337 (1980).
[36]J. S. Hutchinson and R. E. Wyatt, Chem. Phys. Lett. **72**, 378 (1980).